

Article

# Effect of Additives on the Activity of Nickel–Tungsten Sulfide Hydroconversion Catalysts Prepared In Situ from Oil-Soluble Precursors

Mariia Kniazeva <sup>1,\*</sup> and Anton Maximov <sup>1,2</sup>

<sup>1</sup> A.V. Topchiev Institute of Petrochemical Synthesis, Russian Academy of Sciences (TIPS RAS), 119991 Moscow, Russia; max@ips.ac.ru

<sup>2</sup> Department of Petroleum Chemistry and Organic Catalysis, Moscow State University, 119991 Moscow, Russia

\* Correspondence: kniazeva@ips.ac.ru; Tel.: +7-495-647-5927 (ext. 125)

Received: 28 September 2018; Accepted: 5 December 2018; Published: 10 December 2018



**Abstract:** The nickel–tungsten sulfide catalysts for the hydroconversion of hydrocarbons were prepared from oil-soluble nickel and tungsten precursor compounds in situ with the use of silica, alumina, titania, zeolite Y, and amorphous aluminosilicate as additives in a vacuum gas oil medium. It was found that the catalytic activity in hydrocracking depends on the concentration of acid sites in the resulting catalyst. With the use of oxide additives, the dispersion and the promoter ratio of the in situ formed sulfide particles increased in the order  $\text{SiO}_2\text{--Al}_2\text{O}_3\text{--TiO}_2$ . It was noted that the promoter ratio of sulfide particles obtained with the use of aluminosilicate additives depended on their porous structure peculiarities. The use of titanium dioxide as a catalytic system component made it possible to reach high activity in hydrocracking, hydrodearomatization, and hydrodesulfurization, which was comparable to that of a system based on zeolite Y, a highly acidic component.

**Keywords:** in situ catalysts; dispersed catalysts; hydroconversion; vacuum gas oil

## 1. Introduction

Supported sulfide catalysts are currently most widely used in the petroleum refining processes of hydrocracking, hydrodesulfurization, hydrodenitrogenation, etc. [1]. Numerous studies on the use of the sulfide catalysts for fixed-bed hydroprocessing were devoted to the effects of supports and metal precursors on the synthesis, the characterization of active sites, etc. [2–15]. The problems of fixed-bed processes in the case of heavy oil fractions include a high rate of catalysts deactivation due to the presence of local overheating zones caused by highly exothermic reactions and the formation of condensation products and coke deposits, which block both the pores of the support and the catalytically active sites [16,17]. A modern approach to the hydroprocessing of heavy crude oil consists in the use of slurry reactors with meso- or nanosized dispersed-phase catalysts [17–29]. This approach ensures a uniform heat distribution in the reaction zone, a high degree of conversion of raw materials, a decrease in the rate of deactivation due to coking, and the possibility of easy catalyst removal from the reactor [30–32].

Dispersed catalysts, both preliminarily synthesized with the use of supports (ex situ) and in situ formed from water-soluble or oil-soluble metal compounds in the reaction medium, are successfully used in slurry hydroprocesses [17,33–42].

Iron and tungsten carbonyls [43,44], molybdenum and nickel ethylhexanoates [45], molybdenum naphthenate [46], and their combinations [47,48] can be used as precursor salts. In this case, the catalytically active phase is a metal sulfide that is formed from a metal-containing precursor

and sulfur-containing feed components and/or sulfur additives [49]. The active sites in sulfide catalysts are sulfur vacancies at the edges of (Mo)WS<sub>2</sub> slabs [50]. In bimetallic systems the catalytic synergism, for example, of Ni and W is attributed to the formation of Ni–W–S phase where highly dispersed WS<sub>2</sub> crystallites are decorated with Ni, which act as promoter. Thus, this sulfide particles can be denoted as (Ni)WS<sub>2</sub>. In previous publications, it was established that a combination of the oil-soluble precursor salts and elemental sulfur additives makes it possible to form dispersed catalyst, which is highly active in the hydrogenation of diaromatic compounds, that was explained by authors by the formation of above mentioned Ni–W–S active phase [27,44].

As a rule, the cracking activity of these formed sulfides is relatively low, and it manifests itself at temperatures above 420 °C; the activity can be changed with the use of acidic additives [25,26] to form bifunctional catalyst analogue or with the use as the additive traditional supported hydrocracking catalysts [51,52]. It was found that the use of zeolites as additives increases the stability of dispersed sulfide catalysts under hydrocracking conditions and can increase the activity in hydrogenation [25,26]. However, in contrast to traditional supported sulfide catalysts [53–55], the formation of catalysts with the use of oxide material additives directly in the reaction medium and their influence on hydrogenation and hydrocracking reactions in slurry systems are not clearly understood. A number of published papers contain data on the effect of the oxide support on the hydrogenation, cracking, and hydrodesulfurization of model substrates on the traditional supported catalysts under steady-state conditions [56–61]. In particular, it was found that the oxide supports affect the morphology and the degree of sulfidation of sulfide particles formed from precursors due to differences in the electronic interactions of the precursor and the support. It was noted that systems based on aluminum oxide are characterized by a higher activity in hydrogenation, whereas systems with titanium oxide exhibit an increased activity in hydrogenolysis.

In this work, we studied the catalytic systems formed from nickel(II) 2-ethylhexanoate, tungsten hexacarbonyl, and the additives of titania, alumina, silica, and alumina-containing oxide materials (zeolite Y and amorphous aluminosilicate) in situ in a vacuum gas oil medium. We found that the nature and properties of the additives affect the activity of the nickel–tungsten sulfide catalysts formed from oil-soluble precursors in hydroconversion reactions.

## 2. Results and Discussion

The activity of the in situ formed catalysts in the hydroconversion of vacuum gas oil (VGO) was studied in a batch mode at a temperature of 390 °C, an initial hydrogen pressure of 5.0 MPa in the reaction system and under vigorous stirring. Nonhydrotreated VGO whose characteristics are given in Materials and Methods section was used as a starting material. The activity of the systems was evaluated from changes in the fractional composition of the starting material and the degrees of hydrodesulfurization and hydrodearomatization. In the absence of catalysts, the vacuum gas oil did not undergo noticeable changes at 390 °C, a pressure of 5.0 MPa in 10 h. It was also found that, in all of the experiments, no more than 2% gaseous cracking products was formed at 390 °C in the course of hydroconversion on the prepared catalysts.

Figure 1 illustrates the dependence of the degrees of conversion, hydrodearomatization, and hydrodesulfurization of the VGO on the total concentration of acid sites in the in situ generated catalysts separated after the reaction. Note that unmodified sulfide catalysts were characterized by low acidity due to the formation of –SH groups on the surface [13].

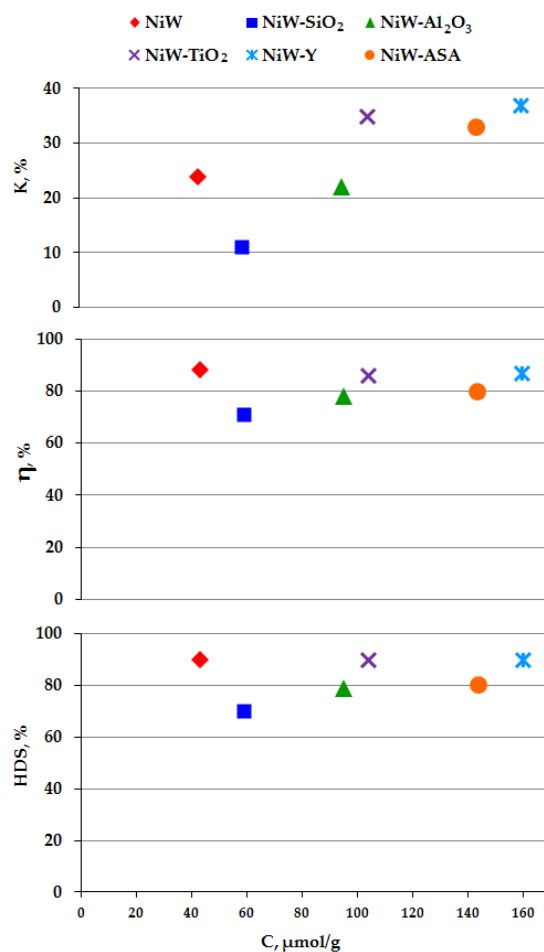


**Figure 1.** Dependence of the degrees of conversion (K), hydrodearomatization ( $\eta$ ), and hydrodesulfurization (HDS) of VGO on the total concentration of acid sites (390 °C, 5.0 MPa, 5 h).

It is well known that, in the case of traditional supported catalysts for hydroprocessing, the acidic properties of the support significantly influenced the distribution of conversion products to increase the yield of light products [15]. A similar effect of the acidity on the degree of VGO conversion was also observed with the in situ formed catalysts from oil soluble precursors and additives, although the activity in both hydrodearomatization and hydrodesulfurization significantly changed in this case. The sulfide catalyst formed from oil-soluble precursors in the absence of modifiers exhibited a high activity in hydrofining (the degrees of dearomatization and hydrodesulfurization were about 90%) and a relatively low activity in hydrocracking (the conversion of VGO into light fractions was about 25%), whereas oxide additives significantly changed the conversion of the raw material. The introduction of silica dramatically decreased the activity in hydrocracking and hydrofining. The introduction of alumina decreased the degrees of hydrodesulfurization and hydrodearomatization, as compared with those of the unmodified system, with the retention of the activity in hydrocracking. The introduction of titania did not affect the activity in the hydrogenation of aromatic compounds and in hydrodesulfurization, but it increased the degree of hydrocracking by 11%. In the series of SiO<sub>2</sub>, Al<sub>2</sub>O<sub>3</sub>, and TiO<sub>2</sub> additives, the catalytic activity in hydrocracking was a linear function of the concentration of acid sites in the resulting catalysts: the VGO conversion increased with the catalyst acidity in the test system. The activity in hydrodearomatization and hydrodesulfurization increased to a much lesser extent.

The use of crystalline and amorphous aluminosilicate additives can increase the acidity of in situ formed catalysts in comparison with the sulfide-based system: upon their addition to the system,

the activity of the resulting catalyst in hydrocracking increased with only a slight decrease in the hydrofining activity (Figure 1).

In spite of a significant difference between the total acid sites concentration of zeolite Y and amorphous aluminosilicate ASA in which the total concentration was three times lower than that in the zeolite (their characteristics are given in Materials and Methods section), the strength of acid sites in almost similar. Both aluminosilicates have practically only weak acid sites. The acid properties of the catalysts separated from the system after the reaction differed insignificantly (Figure 1). This effect may be due to the texture properties of these materials. Amorphous aluminosilicate ASA has a more developed surface area ( $850 \text{ m}^2/\text{g}$ ) furthermore, its structure is a hexagonally ordered pore system with an average pore diameter of  $40 \text{ \AA}$ . Zeolite Y has a three-dimensional porous structure with a channel diameter of  $7.4 \text{ \AA}$  and cavities of  $12 \text{ \AA}$ , its surface area is also developed ( $530 \text{ m}^2/\text{g}$ ) but  $440 \text{ m}^2/\text{g}$  is the micropore area. Thus, the surface acid sites of aluminosilicate (ASA), including those inside the pores, became more accessible compared to Y zeolite after the localization of sulfide particles formed from the precursors. The surface area of NiW-ASA sample was 25% lower compared to ASA. At the same time, in spite of the fact that the acidity of the zeolite-containing catalyst was higher than that of the system with a titania additive, its activity in hydrocracking was higher only slightly (Figure 1).

To explain the experimental data on the activity of the catalysts in hydrodesulfurization and hydrodearomatization, we studied the morphology of the in situ formed catalysts separated after the reaction using transmission electron microscopy (TEM). Note that, in the absence of additives, we observed the formation of the spherical aggregates of sulfide particles with a diameter of about  $50 \text{ nm}$  (Figure 2a). With the use of silica, the agglomerated layered sulfide particles ( $60\text{--}70 \text{ nm}$  in diameter) were localized on the surface of the additive material (Figure 2b). In the case of the NiW- $\text{Al}_2\text{O}_3$  sample, the isolated aggregates of sulfide particles and highly dispersed alumina particles with a diameter of  $15\text{--}25 \text{ nm}$  occurred together with surface oxide particles in the separated catalyst (Figure 2c).

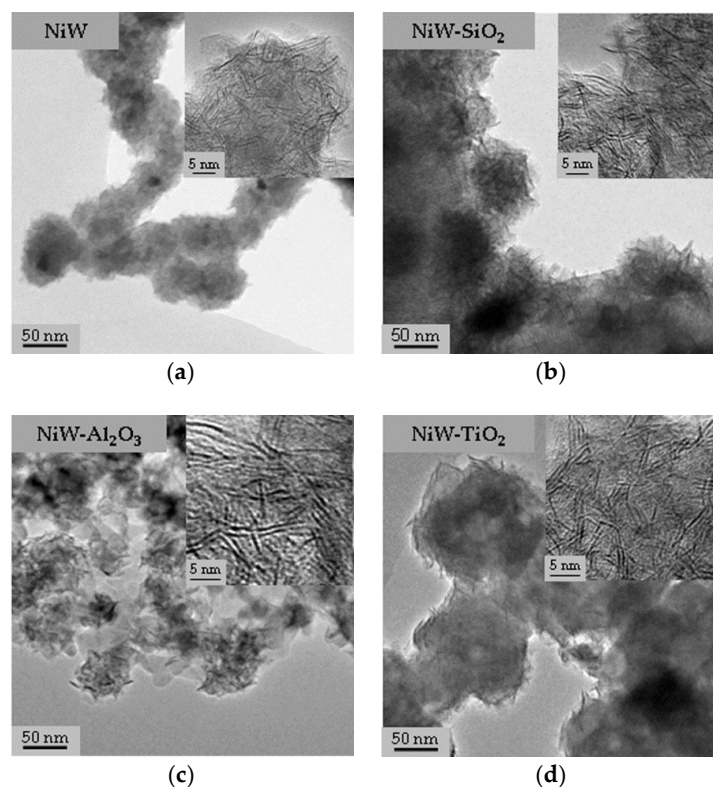


**Figure 2.** TEM micrographs of the catalysts prepared (a) without additives and with oxide additives (b)  $\text{SiO}_2$ , (c)  $\text{Al}_2\text{O}_3$ , (d)  $\text{TiO}_2$  ( $390 \text{ }^\circ\text{C}$ ,  $5.0 \text{ MPa}$ ,  $5 \text{ h}$ ).

According to the TEM data, the separated catalysts based on oxide materials were the agglomerates of sulfide particles localized on the surface of aluminosilicate particles, as in the cases of silica and alumina (Figure 3a,b).

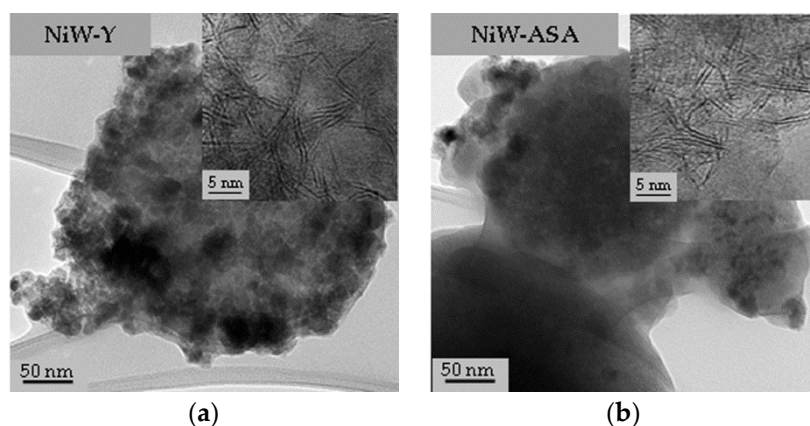


**Figure 3.** TEM micrographs of the catalysts prepared with the aluminosilicate additives (a) Y and (b) ASA (390 °C, 5.0 MPa, 5 h).

With the use of a titania additive, the formation of titanium oxide particles (100–150 nm in diameter) decorated with layered sulfide particles at the edges (Figure 2d) was observed with a small number of individual onion-shaped particle aggregates both on the surface and outside of the oxide; this is a considerable difference between titania and the other additive materials. The resulting catalysts were structurally similar to the classical nickel–tungsten catalysts supported onto TiO<sub>2</sub> [60].

The effects of additives on the morphology parameters of sulfide nanoparticles (the length of a layer and the stacking number) were also found. Based on the statistical analysis carried out after the processing of the microphotographs, the mean length of the sulfide particles and the stacking number were determined (Table 1). Assuming that the particles formed were hexagonally shaped, we calculated the dispersion of (Ni)WS<sub>2</sub> particles using a published procedure [62]. The dispersion increased on going from an unmodified catalyst to the systems formed in the presence of oxides (in the series of SiO<sub>2</sub>–Al<sub>2</sub>O<sub>3</sub>–TiO<sub>2</sub>) due to a decrease in the length and the stacking number of sulfide particles and reached a maximum in the systems based on titanium oxide. Moreover, the aggregation of the individual layered nanoparticles into spherical and onion-shaped aggregates in the titanium oxide was minimal.

**Table 1.** Geometric characteristics of (Ni)WS<sub>2</sub> particles.

Samples	NiW	NiW-SiO <sub>2</sub>	NiW-Al <sub>2</sub> O <sub>3</sub>	NiW-TiO <sub>2</sub>	NiW-Y	NiW-ASA
$\bar{L}^1$	5.1	4.3	3.6	3.3	3.1	4.0
$\bar{N}^2$	1.9	1.8	2.4	2.0	2.1	2.1
D <sup>3</sup>	0.23	0.27	0.32	0.35	0.37	0.30

<sup>1</sup> average length of (Ni)WS<sub>2</sub>, nm. <sup>2</sup> stacking number of (Ni)WS<sub>2</sub>. <sup>3</sup> dispersion of (Ni)WS<sub>2</sub> (see Section 3.2).

Figure 4 shows the dependence of the activity of catalysts in the hydroconversion of VGO on the dispersion. An increase in the dispersion together with a decrease in the fraction of aggregated particles in the order SiO<sub>2</sub>–Al<sub>2</sub>O<sub>3</sub>–TiO<sub>2</sub> led to an increase in the activity in hydrotreating reactions. Highly dispersed sulfide particles (hexagonally shaped) contain more edge and corner active sites [63], which are responsible for the activity in hydrofining reactions.

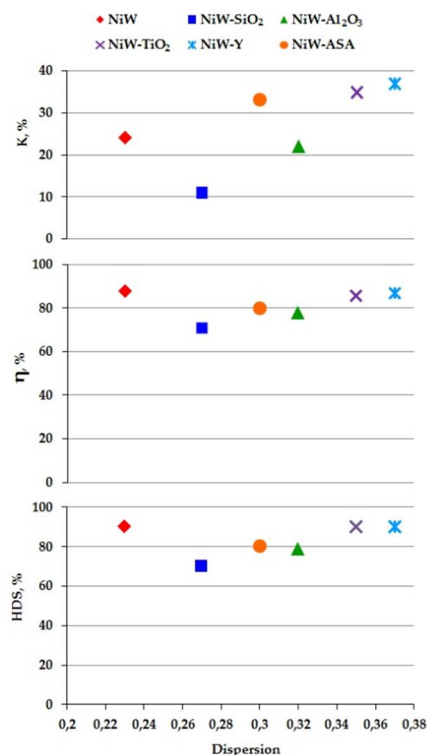


**Figure 4.** Dependence of the degrees of conversion (K), hydrodearomatization ( $\eta$ ), and hydrodesulfurization (HDS) of VGO on the dispersion (390 °C, 5.0 MPa, 5 h).

In bimetallic sulfide catalysts, the edge and corner active sites are responsible for the hydrogenolysis of C–S bonds and the hydrogenation of aromatic hydrocarbons, respectively [64]. It is likely that the reactions of C–S bond hydrogenolysis and the hydrogenation of aromatic hydrocarbons occur at the same active sites. In this case, the rate of a particular process depends on the competitive sorption of reacting molecules because it is well known that sulfur-containing compounds present in the feedstock slow down the hydrogenation reaction [65]. Upon the addition of silica and alumina, a portion of sulfide particles may become inaccessible to reactant molecules due to the orientation of sulfide clusters basal-bonded to the support [66]. In an unmodified catalyst, the aggregates were reversibly destroyed to form a dispersion of layered nanoparticles, and the rate of this process decreased in the presence of silica and alumina. Only in titania, high dispersion was combined with the absence of aggregates, which led to an increase in the hydrogenation activity. The high hydrogenating activity at high acidity of formed NiW-TiO<sub>2</sub> catalytic system also facilitated hydrocracking because the hydrogenation of the aromatic components of VGO resulted in the further rupture of C–C bonds. Therefore, the retention of the catalytic activity of the system formed in the presence of titania in hydrogenation was responsible for an increase in the fraction of hydrocracking products.

The activity of a traditional supported sulfide catalysts also depends on the degree of sulfidation of the catalyst and on the promoter ratio by nickel. A potential change in the activity due to an increase in dispersion can be compensated for by a decrease in the promoter ratio. In this case, an increase in the degree of interaction with the support led to a decrease in the degree of sulfidation, which was associated with the electronic interaction of tungsten and nickel with the support material [60]. The weaker the interaction, the easier the formation of a sulfide phase. The degree of sulfidation essentially depends on temperature, and a nickel sulfide phase (NiS) and an oxosulfide phase (WO<sub>x</sub>S<sub>y</sub>) were formed on the supported systems at 300–400 °C. The higher the degree of its interaction with the support, the more complicated the sulfidation of the oxosulfide phase and the formation of a mixed Ni–W–S phase [67]. Consequently, both the efficiency of sulfidation and the promoter ratio of tungsten disulfide by nickel atoms increased with decreasing the degree of interaction. Data on the composition

of sulfides in the prepared catalysts separated after the reaction were obtained by X-ray photoelectron spectroscopy (XPS). The signals corresponding to the compounds of oxygen, carbon, sulfur, nickel, and tungsten characteristic of nickel–tungsten sulfide catalysts were detected [68–71].

The sulfide, oxysulfide, and oxide forms of tungsten were found in all of the samples from the W 4*f* deconvolution, as exemplified by the spectrum of the NiW sample (Figure 5a) [72]. As evidenced by the binding energies [72] determined from the Ni 2*p* deconvolution (Figure 5b), nickel occurred on the surface in sulfide and oxygen environments in the following three states: a NiS sulfide, a Ni–W–S phase, and a NiO oxide. The S 2*p* deconvolution showed that sulfur predominantly occurred in the sulfide form ( $S^{2-}$ ) and as oxysulfide and sulfate species (Figure 5c) [73].

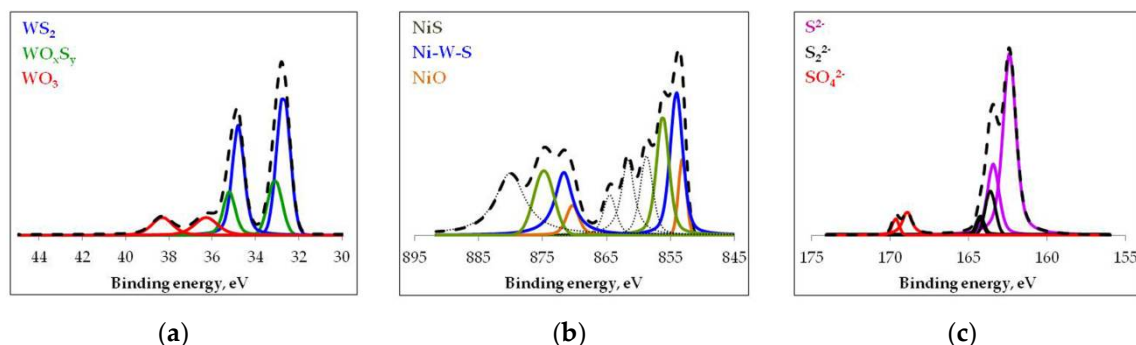


Figure 5. The (a) W 4*f*, (b) Ni 2*p*, and (c) S 2*p* XPS spectra of the NiWS sample.

Table 2 summarizes the relative concentrations of  $WS_2$  and Ni–W–S species found on the catalyst surfaces calculated from the XPS spectra, the effective concentrations of Ni and W, the effective Ni content in Ni–W–S phase and W in  $WS_2$  phase and the promoter ratio in the active phase slab for each sample (see *Physicochemical Analysis of the Additives and Catalysts*). As can be seen, in the presence of the additives, the promoter ratio increased in the order  $SiO_2$ – $Al_2O_3$ – $TiO_2$ ; it is likely that this increase also led to an increase in the hydrogenation activity in this order. At the same time, the fraction of a  $WS_2$  species was substantially lower than that in the unmodified system. This fact confirms the effect of the additives on the formation of the sulfide phase in unsupported catalysts. With the use of oxide additives, the effect caused by the interaction of nickel and tungsten precursors with the surfaces of silica and, to a lesser extent, alumina can decrease the sulfidation efficiency and the formation of a Ni–W–S phase. In the case of the amorphous aluminosilicate and zeolite Y, the promoter ratio was lower to prevent a significant increase in the activity despite the greater dispersion of (Ni) $WS_2$  particles. The electronic interaction of nickel, tungsten, and the oxide materials cannot be responsible for these significant differences in the promoter ratio in the presence of these chemically similar aluminosilicates (Table 2). The porous structure peculiarities of the two aluminosilicates may play a key role in this case. At the initial stage of the in situ formation of a catalyst, the probability of the diffusion of oil-soluble precursor compounds into the wide pores (the widest among the selected additives) of aluminosilicate (ASA) is quite high. Thus, the formation of (Ni) $WS_2$  particles is hindered.

**Table 2.** Results of the surface analysis of the catalysts.

Catalyst	Concentration <sup>1</sup> , Relative %		Effective Concentration <sup>2</sup> , wt %		Effective Content <sup>3</sup> (wt.%)		The Promoter Ratio <sup>4</sup>
	WS <sub>2</sub>	Ni–W–S	W	Ni	WS <sub>2</sub>	Ni–W–S	
NiW	60.1	47.9	9.1	5.8	5.5	2.8	0.51
NiW-SiO <sub>2</sub>	52.8	56.2	6.3	2.6	3.3	1.5	0.45
NiW-Al <sub>2</sub> O <sub>3</sub>	51.8	33.7	3.0	2.6	1.5	0.9	0.60
NiW-TiO <sub>2</sub>	54.3	52.5	7.9	5.1	4.3	2.7	0.63
NiW-ASA	53.2	27.6	8.5	2.3	4.5	0.6	0.13
NiW-Y	52.5	47.6	7.7	3.5	4.0	1.7	0.42

<sup>1</sup> Equations (9) and (10) in Section 3.2. <sup>2</sup> by XPS. <sup>3</sup> Equations (11) and (12) in Section 3.2. <sup>4</sup> Equation (13) in Section 3.2.

### 3. Material and Methods

#### 3.1. Catalyst Preparation Procedure

The catalysts were in situ formed in a reaction medium. For this purpose, the calculated amounts of the oil-soluble precursors of nickel(II) 2-ethylhexanoate (a 78% solution of Ni(C<sub>7</sub>H<sub>15</sub>COO)<sub>2</sub> in 2-ethylhexanoic acid, Aldrich, Aldrich, St. Louis, MO, USA), tungsten hexacarbonyl (99.9% W(CO)<sub>6</sub>, Aldrich, St. Louis, MO, USA), elemental sulfur, and, if required, 1 wt % oxide material were added to the vacuum gas oil. Table 3 characterizes the additives. The tungsten and nickel concentrations in the reaction medium were 0.5 wt %. Titania (TiO<sub>2</sub>, Aldrich, St. Louis, MO, USA) and alumina (Al<sub>2</sub>O<sub>3</sub>, Aldrich, St. Louis, MO, USA) nanopowders (non-porous materials), commercial zeolite Y (CBV 600, Zeolyst, Kansas City, USA) and mesostructured hexagonally ordered MCM-41 type silica (SiO<sub>2</sub>), amorphous, mesostructured hexagonally ordered HMS (Hexagonal Mesoporous Silica) type aluminosilicate (ASA), which were synthesized according to well-known procedures [74,75], were used as additives. The catalyst was sulfidized directly in the reaction medium upon the addition of 2.5 wt % elemental sulfur to vacuum gas oil. The resulting mixture was ultrasonicated for homogenization.

**Table 3.** Characteristics of the additive materials.

Material	Particle Size <sup>1</sup> , nm	S <sub>BET</sub> <sup>2</sup> , m <sup>2</sup> /g	C <sup>3</sup> , μmol/g
SiO <sub>2</sub>	900–1000	1100	13
Al <sub>2</sub> O <sub>3</sub>	15–25	95	157
TiO <sub>2</sub>	100–150	41	77
Y (molar ratio SiO <sub>2</sub> /Al <sub>2</sub> O <sub>3</sub> = 5.2)	400–800	530	532
ASA (molar ratio SiO <sub>2</sub> /Al <sub>2</sub> O <sub>3</sub> = 20)	800–1000	850	170

<sup>1</sup> According to TEM data. <sup>2</sup> Specific surface area found by the low-temperature adsorption of nitrogen.

<sup>3</sup> Total concentration of acid sites according to temperature-programmed desorption (TPD) of ammonia.

#### 3.2. Physicochemical Analysis of the Additives and Catalysts

The texture characteristics of the oxide materials were determined on an ASAP 2020 instrument (Micromeritics, Norcross GA, USA) using the low-temperature adsorption of nitrogen method. The parameters were calculated by the BET method using the instrument software.

Due to the fact that catalytic systems are formed in situ in the reaction medium, their analysis is carried out after separation from the VGO hydroconversion products. Separated catalysts were washed with toluene and cyclohexane and dried in inert atmosphere.

The acidic properties of the oxide materials and the catalysts were determined by the TPD of ammonia on a USGA-101 instrument (Unisit, Moscow, Russia). The sample was placed in a quartz reactor where it was treated in an inert gas flow at 500 °C for 1 h. Saturation with ammonia in a mixture with nitrogen was carried out at 60 °C for 15 min. The physically adsorbed ammonia was removed at 100 °C in a flow of helium at a flow rate of 30 cm<sup>3</sup>/min for 1 h; then, the sample was cooled. To obtain a TPD curve, the sample was heated in a flow of helium (30 cm<sup>3</sup>/min) to 900 °C at a rate of

8 °C/min. The released ammonia was detected with a thermal conductivity detector. Data processing was carried out using the instrument software.

The structure and morphology of the additive materials and the spent catalysts separated after the reaction were studied by high-resolution TEM on a JEM 2100 electron microscope (JEOL, Tokyo, Japan) at an accelerating voltage of 200 kV. Typically, the lengths of at least 500 slabs were measured for each catalyst. To measure the (Ni)WS<sub>2</sub> dispersion, the average fraction of W atoms at the (Ni)WS<sub>2</sub> edge surface was calculated, assuming that the sulfide slabs were perfect hexagons [62]. The presence of a certain number of nickel atoms is not considered. Dispersion (D) was statistically evaluated by dividing the total number of W atoms at the edge surface (We), including corner sites (Wc), by the total number of W atoms (W<sub>T</sub>) using the slab sizes measured in the TEM micrographs:

$$D = \frac{We + Wc}{W_T} \quad (1)$$

$$We = (6 \times n_i - 12) \times \bar{N} \quad (2)$$

$$Wc = 6 \times \bar{N} \quad (3)$$

$$W_T = (3 \times n_i^2 - 3 \times n_i + 1) \times \bar{N}, \quad (4)$$

where  $n_i$  is the number of W atoms along one side of the (Ni)WS<sub>2</sub> slab, as determined by its average length  $\bar{L}$ .

$$\bar{L} = \frac{\sum l_i}{n} \quad (5)$$

where  $l_i$  is a length of each slab.

$$n_i = \frac{10 \times \frac{\bar{L}}{3.2} + 1}{2} \quad (6)$$

and

$$\bar{N} = \frac{\sum n_i N_i}{n}, \quad (7)$$

where  $\bar{N}$  is the average stacking degree and  $n_i$  is the number of stacks in  $N_i$  layers.

The separated catalysts were studied XPS using a PHI 5500 ESCA X-ray photoelectron spectrometer (Physical Electronics, Chanhassen, MN, USA). Nonmonochromatic AlK $\alpha$  radiation ( $h\nu = 1486.6$  eV) with a power of 300 W was used to excite photoemission. Powders were pressed into an indium plate. The diameter of the analysis area was 1.1 mm. The photoelectron peaks were calibrated using the C 1s line of carbon with a binding energy of 284.9 eV. The deconvolution of spectra was performed by a nonlinear least squares method using the Gaussian–Lorentzian function.

We determined the relative concentrations of each species NiS, Ni–W–S, WS<sub>2</sub> etc. for every catalyst. As example, the relative amount of Ni–W–S (%):

$$[\text{Ni–W–S}] = \frac{A_{\text{Ni–W–S}}}{A_{\text{Ni–W–S}} + A_{\text{NiS}} + A_{\text{NiO}}} \times 100, \quad (8)$$

$$[\text{WS}_2] = \frac{A_{\text{WS}_2}}{A_{\text{WS}_2} + A_{\text{WO}_3} + A_{\text{WO}_x\text{S}_y}} \times 100, \quad (9)$$

where  $A_M$  is the peak area of  $M$  species.

The effective Ni content in Ni–W–S phase and W in WS<sub>2</sub> phase:

$$C_{\text{NiWS}} = \frac{[\text{Ni–W–S}] \times C_{\text{Ni}}}{100} \quad (10)$$

$$C_{\text{NiWS}} = \frac{[\text{WS}_2] \times C_{\text{W}}}{100} \quad (11)$$

where  $C_{Ni}$  and  $C_W$  are effective concentrations of Ni and W determined by XPS (wt. %).

The promoter ratio in the active phase slab was determined:

$$\left(\frac{Ni}{W}\right)_{slab} = \frac{C_{Ni-W-S}}{C_{WS_2}} \quad (12)$$

### 3.3. Catalytic Experiment Procedure

The hydroconversion of VGO, whose characteristics are given in Table 4, was carried out in an autoclave batch reactor under vigorous stirring. A mixture, prepared according to Section 3.1 (Catalyst Preparation Procedure) was placed in a 30 mL steel autoclave; the autoclave was purged with nitrogen to remove air and then filled with hydrogen to a pressure of 5.0 MPa. The process temperature was 390 °C, and the reaction time 5 h. The catalyst was separated from the products by centrifugation, and the liquid products were analyzed.

**Table 4.** Characteristics of nonhydrotreated VGO.

Parameter	Test Results, °C
Fractional composition distillation temperature:	
IBP <sup>1</sup>	333
10%	360
50%	437
EBP <sup>2</sup>	537
Sulfur content, wt %	1.86

<sup>1</sup> initial boiling point; <sup>2</sup> end boiling point.

### 3.4. Analysis of Conversion Products

The fractional composition VGO and the products of conversion (gasoline fraction, <180 °C; diesel fraction, 180–360 °C; and residual fraction, >360 °C) was determined by simulated distillation on a KristalLyuks 4000M gas chromatograph (Meta-Khrom, Yoshkar-Ola, Russia) equipped with a flame-ionization detector (FID). The test sample components were separated on an SPB-1 special chromatographic column (dimethylpolysiloxane, 30 m × 0.25 mm) from Supelco, Bellefonte, PA, USA). The chromatograms were processed in an automatic mode. The degree of conversion  $K$  of VGO was determined from the concentrations of residual fractions (>360 °C) in the feed and conversion products.

The concentration of sulfur in the feed and liquid products was determined on a Spectroscan S energy-dispersive X-ray fluorescence analyzer (Spektron, St. Petersburg, Russia) using a standard procedure in accordance with ASTM D4294. The degree of hydrodesulfurization (HDS) was calculated from the sulfur contents of the feed and conversion products.

The aromatic hydrocarbon content was determined by <sup>1</sup>H NMR spectroscopy on an MSL-300 instrument (Bruker, Karlsruhe, Germany) according to ASTM D5292. The high-resolution spectra were measured in solutions in CDCl<sub>3</sub>; the chemical shifts were determined with reference to the residual chloroform signals at 7.27 ppm using the PAPS (Phase Alternating Pulse Sequence) computer program with the subsequent Fourier transform. The spectra were integrated in the ranges of chemical shifts of 0.5–5.0 ppm, which corresponds to hydrogen atoms at aliphatic carbon atoms, and of 5.0–10.0 ppm, which corresponds to hydrogen atoms at aromatic rings. The degree of hydrodearomatization (■) was calculated from changes in the relative concentrations of protons at the aromatic rings in the conversion products and VGO.

## 4. Conclusions

Thus, we found that the hydrocracking activity of the catalysts formed with the use of the SiO<sub>2</sub>, Al<sub>2</sub>O<sub>3</sub>, and TiO<sub>2</sub> oxide additives was a linear function of the concentration of formed catalysts acid sites. The aluminosilicate additives, which are characterized by a high concentration of acid sites, allowed us

to form a catalyst whose activity in hydrocracking was comparable to that of the NiW–TiO<sub>2</sub> system. The dispersion of the sulfide particles formed, the promoter ratio and, correspondingly, the activity in hydrofining increased in the following order of additives: SiO<sub>2</sub>, Al<sub>2</sub>O<sub>3</sub>, and TiO<sub>2</sub>. The promoter ratio of the highly dispersed (Ni)WS<sub>2</sub> particles formed with the use of amorphous aluminosilicate additives was low due to the diffusion of precursor compounds into pores at the initial stage of the in situ catalyst formation.

Based on the experimental results, we arranged the following orders of activity for the prepared catalysts:

NiW-Y  $\approx$  NiW-TiO<sub>2</sub>  $\approx$  NiW-ASA > NiW  $\approx$  NiW-Al<sub>2</sub>O<sub>3</sub> >> NiW-SiO<sub>2</sub> for hydrocracking;  
 NiW  $\approx$  NiW-Y  $\approx$  NiW-TiO<sub>2</sub> > NiW-ASA > NiW-Al<sub>2</sub>O<sub>3</sub> > NiW-SiO<sub>2</sub> for hydrodearomatization; and  
 NiW-Y = NiW-TiO<sub>2</sub> = NiW > NiW-ASA  $\approx$  NiW-Al<sub>2</sub>O<sub>3</sub> > NiW-SiO<sub>2</sub> for hydrodesulfurization.

Thus, at this stage of study titania dioxide is the most promising material from the list of tested. In the presence TiO<sub>2</sub> it was managed to form nickel-tungsten sulfide catalyst characterized by a high dispersion and promoter ratio, as well as high acidity, that in total ensures the efficiency in hydroprocesses.

**Author Contributions:** Conceptualization, M.K. and A.M.; methodology, M.K.; investigation, M.K.; data curation, M.K.; writing—original draft preparation, M.K.; writing—review and editing, A.M.; supervision, A.M.; project administration, A.M.

**Acknowledgments:** This work was carried out within the State Program of TIPS RAS and has been supported by the Russian Science Foundation, the agreement no. 17-73-30046.

**Conflicts of Interest:** The authors declare no conflict of interest.

## References

1. Marafi, M.; Stanislaus, A.; Furimsky, E. Hydroprocessing technology. In *Handbook of Spent Hydroprocessing Catalysts*, 2nd ed.; Elsevier: Amsterdam, The Netherlands, 2017; pp. 27–66, ISBN 978-0-444-63881-6.
2. Furimsky, E. Spent refinery catalysts: Environment, safety and utilization. *Catal. Today* **1996**, *30*, 223–286. [[CrossRef](#)]
3. Breyse, M.; Furimsky, E.; Kasztelan, S.; Lacroix, M.; Perot, G. Hydrogen activation by transition metal sulfides. *Catal. Rev. Sci. Eng.* **2002**, *44*, 651–735. [[CrossRef](#)]
4. Kasztelan, S.; MacGarvey, B. Hydrogen Content and Hydrogenation Activity of MoS<sub>2</sub>/ $\gamma$ -Al<sub>2</sub>O<sub>3</sub> and  $\gamma$ -Al<sub>2</sub>O<sub>3</sub> Mechanical Mixtures. *J. Catal.* **1994**, *147*, 476–483. [[CrossRef](#)]
5. Raybaud, P. Understanding and predicting improved sulfide catalysts: Insights from first principles modeling. *Appl. Catal. A Gen.* **2007**, *322*, 76–91. [[CrossRef](#)]
6. MacGarvey, B.; Kasztelan, S. An Investigation of the Reduction Behavior of MoS<sub>2</sub>/Al<sub>2</sub>O<sub>3</sub> and the Subsequent Detection of Hydrogen on the Surface. *J. Catal.* **1994**, *148*, 149–156. [[CrossRef](#)]
7. Breyse, M.; Bennett, B.A.; Chadwick, D.; Vrinat, M. Structure and HDS Activity of Co-Mo Catalysts: A Comparison of Alumina and Carbon Supports. *Bull. Soc. Chim. Belg.* **1981**, *90*, 1271–1278. [[CrossRef](#)]
8. Bouwens, S.M.A.M.; van Zon, F.B.M.; van Dijk, M.P.; van der Kraan, A.M.; de Beer, V.H.J.; van Veen, J.A.R.; Koningsberger, D.C. On the Structural Differences Between Alumina-Supported Comos Type I and Alumina-, Silica-, and Carbon-Supported Comos Type II Phases Studied by XAFS, MES, and XPS. *J. Catal.* **1994**, *146*, 375–393. [[CrossRef](#)]
9. Louwers, S.P.A.; Prins, R. Ni EXAFS studies of the Ni–Mo–S structure in carbon-supported and alumina-supported Ni–Mo catalysts. *J. Catal.* **1992**, *133*, 94–111. [[CrossRef](#)]
10. Dugulan, A.I.; Craje, M.W.J.; Overweg, A.R.; Kearley, G.J. The evolution of the active phase in CoMo/C hydrodesulfurization catalysts under industrial conditions: A high-pressure Mössbauer emission spectroscopy study. *J. Catal.* **2005**, *229*, 276–282. [[CrossRef](#)]
11. Dufresne, P. Hydroprocessing catalysts regeneration and recycling. *Appl. Catal. A Gen.* **2007**, *322*, 67–75. [[CrossRef](#)]

12. Brorson, M.; Carlson, A.; Topsoe, H. The morphology of MoS<sub>2</sub>, WS<sub>2</sub>, Co–Mo–S, Ni–Mo–S and Ni–W–S nanoclusters in hydrodesulfurization catalysts revealed by HAADF-STEM. *Catal. Today* **2007**, *123*, 31–36. [[CrossRef](#)]
13. Topsoe, H. The role of Co–Mo–S type structures in hydrotreating catalysts. *Appl. Catal. A Gen.* **2007**, *322*, 3–8. [[CrossRef](#)]
14. Besenbacher, F.; Brorson, M.; Clausen, B.S.; Helveg, S.; Hinnemann, B.; Kibsgard, J.; Lauristen, J.V.; Moses, P.G.; Norskov, J.K.; Topsoe, H. Recent STM, DFT and HAADF-STEM studies of sulfide-based hydrotreating catalysts: Insight into mechanistic, structural and particle size effects. *Catal. Today* **2008**, *130*, 86–96. [[CrossRef](#)]
15. Eijssbouts, S.; Mayo, S.W.; Fujita, K. Unsupported transition metal sulfide catalysts: From fundamentals to industrial application. *Appl. Catal. A Gen.* **2007**, *322*, 58–66. [[CrossRef](#)]
16. Furimsky, E. Catalyst deactivation. In *Catalyst for Upgrading Heavy Petroleum Feed*; Elsevier Science: Amsterdam, The Netherlands, 2007; pp. 141–216, ISBN 978-0-444-53084-4.
17. Nguyen, M.T.; Nguyen, N.T.; Cho, J.; Parka, C.; Parka, S.; Jung, J.; Lee, C.W. A review on the oil-soluble dispersed catalyst for slurry-phase hydrocracking of heavy oil. *J. Ind. Eng. Chem.* **2016**, *43*, 1–12. [[CrossRef](#)]
18. Sahu, R.; Song, B.J.; Im, J.S.; Jeon, Y.-P.; Lee, C.W. A review of recent advances in catalytic hydrocracking of heavy residues. *J. Ind. Eng. Chem.* **2015**, *27*, 12–24. [[CrossRef](#)]
19. Go, K.S.; Kim, Y.K.; Kwon, E.H.; Nho, N.S. Characteristics of slurry-phase hydrocracking for vacuum residue with reaction temperature and concentrations of MoS<sub>2</sub> dispersed catalysts. *Catal. Today* **2018**, *305*, 92–101. [[CrossRef](#)]
20. Kim, S.-H.; Kim, K.-D.; Lee, Y.-K. Effects of dispersed MoS<sub>2</sub> catalysts and reaction conditions on slurry phase hydrocracking of vacuum residue. *J. Catal.* **2017**, *347*, 127–137. [[CrossRef](#)]
21. Nguyen, T.M.; Jung, J.; Lee, C.W.; Cho, J. Effect of asphaltene dispersion on slurry-phase hydrocracking of heavy residual hydrocarbons. *Fuel* **2018**, *214*, 174–186. [[CrossRef](#)]
22. Khadzhiev, S.N.; Kadiev, K.M.; Zhigalina, O.M.; Kadieva, M.K.; Khmelenin, D.N. Structure and Properties of Molybdenum Sulfide Nanoparticles Synthesized In situ in the Hydroconversion Process. *Pet. Chem.* **2015**, *55*, 655–662. [[CrossRef](#)]
23. Sizova, I.A.; Maksimov, A.L. Nickel–molybdenum Sulfide Naphthalene Hydrogenation Catalysts Synthesized by the In situ Decomposition of Oil-soluble Precursors. *Pet. Chem.* **2017**, *57*, 595–599. [[CrossRef](#)]
24. Khadzhiev, S.N.; Kadiev, K.M.; Kadieva, M.K. Synthesis and Properties of Nanosized Systems as Efficient Catalysts for Hydroconversion of Heavy Petroleum Feedstock. *Pet. Chem.* **2014**, *54*, 323–346. [[CrossRef](#)]
25. Onishchenko, M.I.; Kulikov, A.B.; Maksimov, A.L. Application of Zeolite Y-Based Ni–W Supported and In Situ Prepared Catalysts in the Process of Vacuum Gas Oil Hydrocracking. *Pet. Chem.* **2017**, *57*, 1287–1294. [[CrossRef](#)]
26. Onishchenko, M.I.; Maksimov, A.L. Activity of Supported and In Situ Synthesized Beta Zeolite Catalysts in the Hydrocracking of Vacuum Gas Oil. *Pet. Chem.* **2018**, *58*, 651–658. [[CrossRef](#)]
27. Maximov, A.L.; Sizova, I.A.; Khadzhiev, S.N. Catalysis in a Dispersion Medium for the Hydrogenation of Aromatics and Hydrodearomatization in Oil Refining. *Pure Appl. Chem.* **2017**, *89*, 1145–1155. [[CrossRef](#)]
28. Shuyi, Z.; Wenan, D.; Hui, L.; Dong, L.; Guohe, Q. Slurry-phase Residue Hydrocracking with Dispersed Nickel Catalyst. *Energy Fuels* **2008**, *22*, 3583–3586. [[CrossRef](#)]
29. Dong, L.; Hui, D.; Jichang, Z.; Guohe, Q. Reverse Microemulsion Synthesis and Characterization of Nano Nickel Sulfide Catalyst for Residue Slurry-Phase Hydrocracking. *Energy Fuels* **2015**, *29*, 3353–3358. [[CrossRef](#)]
30. Zhang, S.; Liu, D.; Deng, W.; Que, G. A Review of Slurry-Phase Hydrocracking Heavy Oil Technology. *Energy Fuels* **2007**, *21*, 3057–3062. [[CrossRef](#)]
31. Khadzhiev, S.N. Nanoheterogeneous catalysis: A New Sector of Nanotechnologies in Chemistry and Petroleum Chemistry (A Review). *Pet. Chem.* **2011**, *51*, 1–15. [[CrossRef](#)]
32. Khadzhiev, S.N. Nanoheterogeneous catalysis: Definition, State, and Research Prospects (Review). *Pet. Chem.* **2016**, *56*, 465–479. [[CrossRef](#)]
33. Hur, Y.G.; Lee, D.-W.; Lee, K.-Y. Hydrocracking of Vacuum Residue Using NiWS(x) Dispersed Catalysts. *Fuel* **2016**, *185*, 794–803. [[CrossRef](#)]
34. Nguyen, T.S.; Tayakout-Fayolle, M.; Lacroix, M.; Gotteland, D.; Aouine, M.; Bacaud, R.; Afanasiev, P.; Geantet, C. Promotion Effects With Dispersed Catalysts for Residue Slurry Hydroconversion. *Fuel* **2015**, *160*, 50–56. [[CrossRef](#)]

35. Maity, S.K.; Ancheyta, J.; Alonso, F.; Rayo, P. Hydrodesulfurization activity of used hydrotreating catalysts. *Fuel Proc. Tech.* **2013**, *106*, 453–459. [[CrossRef](#)]
36. Del Bianco, A.; Panariti, N.; Di Carlo, S.; Beltrame, P.L.; Carniti, P. New Developments in Deep Hydroconversion of Heavy Oil Residues with Dispersed Catalysts. 2. Kinetic Aspects of Reaction. *Energy Fuels* **1994**, *8*, 593–597. [[CrossRef](#)]
37. Ortiz-Moreno, H.; Ramírez, J.; Cuevas, R.; Marroquín, G.; Ancheyta, J. Heavy oil upgrading at moderate pressure using dispersed catalysts: Effects of temperature, pressure and catalytic precursor. *Fuel* **2012**, *100*, 186–192. [[CrossRef](#)]
38. Jeon, S.G.; Na, J.-G.; Ko, C.H.; Lee, K.B.; Rho, N.S.; Park, S.B. A new approach for preparation of oil-soluble bimetallic dispersed catalyst from layered ammonium nickel molybdate. *Mater. Sci. Eng. B* **2011**, *176*, 606–610. [[CrossRef](#)]
39. Liu, D.; Kong, X.; Li, M.; Que, G. Study on a Water-Soluble Catalyst for Slurry-Phase Hydrocracking of an Atmospheric Residue. *Energy Fuels* **2009**, *23*, 958–961. [[CrossRef](#)]
40. Angeles, M.J.; Leyva, C.; Ancheyta, J.; Ramírez, S. A review of experimental procedures for heavy oil hydrocracking with dispersed catalyst. *Catal. Today* **2014**, *220–222*, 274–294. [[CrossRef](#)]
41. Rispoli, G.F.; Bellussi, G. Process for the Refining of Crude Oil. E.P. Patent No. 2,633,002, 4 September 2013.
42. Bellussi, G.; Rispoli, G.; Landoni, A.; Millini, R.; Molinari, D.; Montanari, E.; Moscotti, D.; Pollesel, P. Hydroconversion of heavy residues in slurry reactors: Developments and perspectives. *J. Catal.* **2013**, *308*, 189–200. [[CrossRef](#)]
43. Cyr, T.; Lewkowicz, L.; Ozum, B. Hydrocracking Process Involving Colloidal Catalyst Formed In Situ. U.S. Patent No. 5,578,197, 26 November 1996.
44. Sizova, I.A.; Kulikov, A.B.; Onishchenko, M.I.; Serdyukov, S.I.; Maksimov, A.L. Synthesis of Nickel–tungsten Sulfide Hydrodearomatization Catalysts by the Decomposition of Oil-soluble Precursors. *Pet. Chem.* **2016**, *56*, 44–50. [[CrossRef](#)]
45. Strausz, O.P. Process for Hydrocracking Heavy Oil. U.S. Patent No. 6,068,758, 30 May 2000.
46. Aldridge, C.L.; Bearden, R.J. Hydroconversion of Heavy Hydrocarbons. U.S. Patent No. 4,066,530, 3 January 1978.
47. Zhou, B.; Zhou, Z.; Wu, Z. Hydrocarbon-Soluble, Bimetallic Catalyst Precursors and Methods for Making Same. U.S. Patent No. 7,842,635, 30 November 2010.
48. Panariti, N.; Del Bianco, A.; Del Piero, G.; Marchionna, M. Petroleum residue upgrading with dispersed catalysts: Part 1. Catalysts activity and selectivity. *Appl. Catal. A Gen.* **2000**, *204*, 203–213. [[CrossRef](#)]
49. Du, H.; Li, M.; Ren, Y.; Duan, Y. Slurry-phase hydrocracking of heavy oil and model reactant: Effect of dispersed Mo catalyst. *Appl. Petrochem. Res.* **2015**, *5*, 89–98. [[CrossRef](#)]
50. Daage, M.; Chianelli, R.R. Structure-Function Relations in Molybdenum Sulfide Catalysts: The “Rim-Edge” Model. *J. Catal.* **1994**, *149*, 414–427. [[CrossRef](#)]
51. Kennepohl, D.; Sanford, E. Conversion of Athabasca Bitumen with Dispersed and Supported Mo-Based Catalysts as a Function of Dispersed Catalyst Concentration. *Energy Fuels* **1996**, *10*, 229–234. [[CrossRef](#)]
52. Bellussi, G.; Rispoli, G.; Molinari, D.; Landoni, A.; Pollesel, P.; Panariti, N.; Millini, R.; Montanari, E. The role of MoS<sub>2</sub> nano-slabs in the protection of solid cracking catalysts for the total conversion of heavy oils to good quality distillates. *Catal. Sci. Technol.* **2013**, *3*, 176–182. [[CrossRef](#)]
53. Ferraz, S.G.A.; Santos, B.M.; Zotin, F.M.Z.; Araujo, L.R.R.; Zotin, J.L. Influence of Support Acidity of NiMo Sulfide Catalysts for Hydrogenation and Hydrocracking of Tetralin and Its Reaction Intermediates. *Ind. Eng. Chem. Res.* **2015**, *54*, 2646–2656. [[CrossRef](#)]
54. Luck, F. A review of support effects on the activity and selectivity of hydrotreating catalysts. *Bull. Soc. Chim. Belg.* **1991**, *100*, 781–800. [[CrossRef](#)]
55. Breyse, M.; Afanasiev, P.; Geantet, C.; Vrinat, M. Overview of support effects in hydrotreating catalysts. *Catal. Today.* **2003**, *86*, 5–16. [[CrossRef](#)]
56. Nishijima, A.; Shimada, H.; Sato, T.; Yoshimura, Y.; Hiraishi, J. Support effects on hydrocracking and hydrogenation activities of molybdenum catalysts used for upgrading coal-derived liquids. *Polyhedron* **1986**, *5*, 243–247. [[CrossRef](#)]
57. Shimada, H.; Sato, T.; Yoshimura, Y.; Hiraishi, J.; Nishijima, A. Support effect on the catalytic activity and properties of sulfided molybdenum catalysts. *J. Catal.* **1988**, *110*, 275–284. [[CrossRef](#)]

58. Castillo-Villalón, P.; Ramírez, J.; Cuevas, R.; Vázquez, P.; Castañeda, R. Influence of the support on the catalytic performance of Mo, CoMo, and NiMo catalysts supported on Al<sub>2</sub>O<sub>3</sub> and TiO<sub>2</sub> during the HDS of thiophene, dibenzothiophene, or 4,6-dimethyldibenzothiophene. *Catal. Today* **2015**, *259*, 140–149. [[CrossRef](#)]
59. Ng, K.Y.S.; Gulari, E. Molybdena on titania: II. Thiophene hydrodesulfurization activity and selectivity. *J. Catal.* **1985**, *95*, 33–40. [[CrossRef](#)]
60. Vissenberg, M.J.; der Meer, Y.; Hensen, E.J.M.; de Beer, V.H.J.; van der Kraan, A.M.; van Santen, R.A.; van Veen, J.A.R. The Effect of Support Interaction on the Sulfidability of Al<sub>2</sub>O<sub>3</sub>- and TiO<sub>2</sub>-Supported CoW and NiW Hydrodesulfurization Catalysts. *J. Catal.* **2001**, *198*, 151–163. [[CrossRef](#)]
61. Shimada, H. Morphology, Dispersion and Catalytic Functions of Supported Molybdenum Sulfide Catalysts for Hydrotreating Petroleum Fractions. *J. Jpn. Pet. Inst.* **2016**, *59*, 46–58. [[CrossRef](#)]
62. Kasztelan, S.; Toulhoat, H.; Grimblot, J.; Bonnelle, J.P. A geometrical model of the active phase of hydrotreating catalysts. *Appl. Catal.* **1984**, *13*, 127–159. [[CrossRef](#)]
63. Vradman, L.; Landau, M.V. Structure–Function Relations in Supported Ni–W Sulfide Hydrogenation Catalysts. *Catal. Lett.* **2001**, *77*, 47–54. [[CrossRef](#)]
64. Stanislaus, A.; Cooper, B.H. Aromatic Hydrogenation Catalysis: A Review. *Catal. Rev. Sci. Eng.* **1994**, *36*, 75–123. [[CrossRef](#)]
65. Ichihara, A.; Itoh, T.; Hino, T.; Nomura, M.; Qi, P.; Kabe, T. Effects of Solvents on Deep Hydrodesulfurization of Benzothiophene and Dibenzothiophene. *J. Catal.* **1993**, *140*, 184–189. [[CrossRef](#)]
66. Shimada, H. Morphology and orientation of MoS<sub>2</sub> clusters on Al<sub>2</sub>O<sub>3</sub> and TiO<sub>2</sub> supports and their effect on catalytic performance. *Catal. Today* **2003**, *86*, 17–29. [[CrossRef](#)]
67. Hensen, E.J.M.; van der Meer, Y.; van Veen, J.A.R.; Niemantsverdriet, J.W. Insight into the formation of the active phases in supported NiW hydrotreating catalysts. *Appl. Catal. A Gen.* **2007**, *322*, 16–32. [[CrossRef](#)]
68. Díaz de León, J.N.; Antunes-García, J.; Alonso-Nuñez, G.; Zepeda, T.A.; Galvan, D.H.; de los Reyes, J.A.; Fuentes, S. Support effects of NiW hydrodesulfurization catalysts from experiments and DFT calculations. *Appl. Catal. B Environ.* **2018**, *238*, 480–490. [[CrossRef](#)]
69. López-Benítez, A.; Berhault, G.; Burel, L.; Guevara-Lara, A. Novel NiW hydrodesulfurization catalysts supported on Sol-Gel Mn-Al<sub>2</sub>O<sub>3</sub>. *J. Catal.* **2017**, *354*, 197–212. [[CrossRef](#)]
70. Palcheva, R.; Dimitrov, L.; Tyuliev, G.; Spojakina, A.; Jiratova, K. TiO<sub>2</sub> nanotubes supported NiW hydrodesulfurization catalysts: Characterization and activity. *Appl. Surf. Sci.* **2013**, *265*, 309–316. [[CrossRef](#)]
71. Pereyma, V.Y.; Klimov, O.V.; Prosvirin, I.P.; Gerasimov, E.Y.; Yashnik, S.A.; Noskov, A.S. Effect of thermal treatment on morphology and catalytic performance of NiW/Al<sub>2</sub>O<sub>3</sub> catalysts prepared using citric acid as chelating agent. *Catal. Today* **2018**, *305*, 162–170. [[CrossRef](#)]
72. Tayeb, K.; Lamonier, C.; Lancelot, C.; Fournier, M.; Bonduelle-Skrzypczak, A.; Bertonici, F. Active phase genesis of NiW hydrocracking catalysts based on nickel salt heteropolytungstate: Comparison with reference catalyst. *Appl. Catal. B Environ.* **2012**, *126*, 55–63. [[CrossRef](#)]
73. Ninh, T.K.T.; Laurenti, D.; Leclerc, E.; Vrinat, M. Support effect for CoMoS and CoNiMoS hydrodesulfurization catalysts prepared by controlled method. *Appl. Catal. A Gen.* **2014**, *487*, 210–218. [[CrossRef](#)]
74. Silvestre-Albero, J.; Sepulveda-Escribano, A.; Reinoso, F.R. Preparation and characterization of zinc containing MCM-41 spheres. *Microporous Mesoporous Mater.* **2008**, *113*, 362–369. [[CrossRef](#)]
75. Chiranjeevi, T.; Kumaran, G.M.; Gupta, J.K.; Murali, D.G. Synthesis and characterization of acidic properties of Al-HMS materials of varying Si/Al ratios. *Termochim. Acta* **2006**, *443*, 87–92. [[CrossRef](#)]

